Academic Journal of Science and Technology
ISSN: 2771-3032 | Vol. 10, No. 3, 2024

A Prognosis and Immunological Study of Cellular Aging Related lncRNAs in Lung Adenocarcinoma

Kaiwei Yang, Baixue Li, Yi Liu

School of Chemical Engineering, Sichuan University of Science & Engineering, Zigong, China

Abstract: Background: Recently, cellular senescence has been recognized as a novel hallmark of cancer. However, the mechanisms that control cellular senescence remain poorly understood. This study seeks to discover long non-coding RNAs (lncRNAs) that are linked to senescence and can predict outcomes in lung adenocarcinoma (LUAD) patients. Methods: Using RNA sequencing data from the Cancer Genome Atlas Lung Adenocarcinoma (TCGA-LUAD) and senescence genes from the CellAge database, a group of lncRNAs related to senescence was initially identified. Subsequently, through univariate and multivariate Cox regression analyses, a senescence-related lncRNA signature (SenLncSig) linked to the prognosis of LUAD was developed. LUAD patients were categorized into high-risk and low-risk groups based on the median risk score of SenLncSig. Kaplan-Meier analysis was employed to assess differences in overall survival (OS) between these subgroups. Additionally, disparities in Gene Set Enrichment Analysis (GSEA), immune infiltration, scores from the tumor immune dysfunction and exclusion (TIDE) module, and choices of chemotherapy and targeted therapy were also evaluated between the high-risk and low-risk groups. Results: Based on univariate and multivariate Cox regression analyses, we established a prognostic model composed of seven senescence-related lncRNAs, named SenLncSig, which includes AL031775.2, AC026355.1, AL365181.2, AC090559.1, AL606489.1, AL513550.1, and C20orf197. This model divides patients into high-risk and low-risk groups, with the high-risk group showing significantly shorter overall survival compared to the low-risk group, with a hazard ratio (HR) of 1.326. The predictive accuracy of SenLncSig was validated through ROC curves and principal component analysis (PCA). Additionally, we developed an intuitive survival prediction tool that combines SenLncSig with clinical pathological features to assess patients' overall survival (OS). Enrichment analysis (GSEA) revealed that SenLncSig is involved in multiple pathways related to tumor immune modulation. Risk model analysis indicated significant differences between the high and low-risk groups in terms of immune status and responses to immunotherapy, chemotherapy, and targeted therapy. Conclusion: In this study, a lncRNA signature named as SenLncSig was developed that not only identifies the senescence phenotype and predicts prognosis but also has the capability to forecast the response of LUAD to immunotherapy.

1. Introduction

According to the GLOBOCAN 2018 statistics, lung cancer has become the most common malignant tumor globally, with high incidence and mortality rates (Bray et al., 2018). Additionally, non-small cell lung cancer (NSCLC) accounts for over 85% of lung cancer cases. The most common histological subtypes of NSCLC are lung squamous cell carcinoma (LUSC) and lung adenocarcinoma (LUAD). Moreover, the complex molecular mechanisms of lung cancer pose significant challenges to treatment, as targeted therapies may be ineffective for some patients (Hoang et al., 2022; West et al., 2012). Thus, identifying new biomarkers for lung adenocarcinoma or lung squamous cell carcinoma is crucial for aiding treatment decisions and guiding personalized prognosis. In China, lung cancer has the highest incidence among malignant tumors, with lung adenocarcinoma accounting for about 40% of lung cancer cases. Surgical resection of early-stage non-small cell lung cancer provides a good prognosis, with a 5-year survival rate of 70-90% (Stage I). However, most patients (about 75%) are diagnosed at a late stage (Stage III/IV), and their survival rates are very low (Miranda-Filho et al., 2019).

Long non-coding RNAs (lncRNAs) are RNA molecules longer than 200 nucleotides that do not have the capacity to encode proteins. Initially, lncRNAs were considered byproducts of the transcription process and were thought to lack practical biological functions, hence they were not given much attention. However, advances in chip technology and bioinformatics have led to the recognition of the significant roles lncRNAs play in biological processes, particularly in pre-transcriptional regulation, post-transcriptional regulation, and epigenetic regulation (Serviss et al., 2014; Zhang et al., 2020). Further research has revealed a close relationship between the occurrence, development, metastasis, and recurrence of tumors and the differential expression of lncRNAs, making them a new focus in cancer research (Silva et al., 2015). Due to their tissue-specific expression, lncRNAs have the potential to serve as novel, specific cancer biomarkers and hold potential for use in auxiliary cancer diagnostics (Do and Kim, 2018). LncRNA detection methods are simple and quick, effectively increasing the likelihood of detecting diseases in patients. Combined with other diagnostic methods, they can aid in the early detection and treatment of tumors. Given the limitations of traditional cancer diagnostic methods, lncRNAs, as more specific and sensitive diagnostic indicators, are expected to significantly improve the accuracy of cancer diagnoses.

LncRNAs have shown potential to enhance diagnostic specificity and sensitivity as specific tumor biomarkers. Abnormally expressed lncRNAs in the serum, particularly those originating from specific tumors, offer higher diagnostic accuracy (Yuan et al., 2020). In lung adenocarcinoma tissues, the expression levels of certain lncRNAs are upregulated; these RNA molecules can act both as oncogenes and tumor suppressor genes, influencing the onset, development, and prognosis of the tumor (Jin et al., 2020). In-depth research on lncRNAs not only helps us better understand the pathogenesis and progression of lung adenocarcinoma but also provides vital information for

developing new treatment methods and mechanisms. Therefore, in lung adenocarcinoma research, lncRNAs will play an indispensable role and have great potential to serve as an important bridge connecting the understanding of disease mechanisms and the discovery of treatment methods.

Cellular senescence is a stable cell cycle arrest program, responding to various internal and external stimuli to eliminate senescent cells and maintain bodily homeostasis. Cellular senescence is primarily caused by the gradual shortening of telomeres, changes in telomere structure, mitosis, oncogene activation, ionizing radiation, oxidation, genotoxic stress, epigenetic alterations, chromatin disarray, protein homeostasis disorders, mitochondrial dysfunction, inflammation, tissue damage signaling, and effects of radiotherapy or chemotherapy (Lecot et al., 2016; Schosserer et al., 2017). Both cancer and aging are driven by the accumulation of cellular damage. Previous studies have shown that aging has both advantages and disadvantages in the process of tumor development and is considered an example of the dichotomy of multiple effects in the evolutionary process (Campisi, 2013). Conversely, aging drives senescent cells into a permanent cell cycle arrest to maintain tissue homeostasis and prevent tumor formation. However, when senescent cells are not cleared by the immune system and accumulate, cellular senescence can produce harmful outcomes, promoting tumor occurrence, development, invasion, and metastasis through various pathways.

The phenotypic changes during cellular senescence are controlled by the changes in specific proteins expressed. These processes are mainly regulated by proteins that link DNA and RNA and various non-coding RNAs, including long non-coding RNAs (lncRNAs). LncRNA XIST is downregulated in aging cells and inhibits the proliferation and promotes apoptosis of NSCLC cells by triggering cell necrosis mediated by the miR-335/SOD2/ROS signaling pathway, thereby inhibiting the progression of NSCLC (Xu et al., 2020). LncRNA H19 regulates the imprinting of the gene cluster containing H19 and Insulin-like Growth Factor 2 (IGF2). Both IGF2 and H19 are associated with growth, proliferation, cell cycle, apoptosis, and aging. LncRNA H19 is also highly expressed in cancer, promoting epithelial-mesenchymal transition and enhancing cancer cell proliferation and metastasis by inhibiting the function of miR-200a and upregulating the expression of ZEB1 and ZEB2 (Shi et al., 2020). In summary, lncRNAs can characterize cellular senescence and serve as an important tool for determining the prognosis of lung adenocarcinoma patients.

2. Materials and Methods

2.1. Dataset and sample extraction

The RNA sequencing data, clinical details, and mutations for lung adenocarcinoma (LUAD) were obtained from The Cancer Genome Atlas Lung Adenocarcinoma (TCGA-LUAD) database (https://portal.gdc.cancer.gov/). Initially, data for 539 LUAD patients were collected. Patients who had incomplete follow-up information, a survival time of less than 30 days, or were missing complete clinicopathological data were excluded from further analysis, resulting in a final cohort of 448 patients. Additionally, 279 senescence-related genes identified through gene manipulation experiments were downloaded from the CellAge online database (http://genomics.senescence.info/cells) (Avelar et al., 2020).

2.2. Differentially expressed genes (DEGs) of cellular senescence in LUAD and normal tissue

A log2 fold change absolute value greater than 1 and a false detection rate (FDR) of less than 0.05 were criteria set to identify differentially expressed genes (DEGs) between 539 tumor samples and 59 normal samples. The DEGs were visualized using the R package limma. Enrichment analysis of these DEGs was conducted utilizing the Kyoto Encyclopedia of Gene and Genome (KEGG) and Gene Ontology (GO).

2.3. Identification of a lncRNAs senescence related signature (SenLncSig) associated with LUAD prognosis

A gene expression network involving senescence-related lncRNA-mRNA co-expression was established using a Pearson correlation coefficient absolute value greater than 0.3 and a p-value less than 0.001 to pinpoint senescence-related lncRNAs. Visualization of the lncRNA-mRNA co-expression network was achieved through a Sankey diagram created with the R package ggalluvial and Cytoscape software (version 3.7.2). Initially, univariate Cox regression analysis was utilized to determine lncRNAs linked to LUAD prognosis. These lncRNAs were then used in a multivariate Cox regression analysis to develop a prognostic model for LUAD, which was named SenLncSig. The risk score for this model was calculated with the formula: risk score = explncRNA1 × coef lncRNA1 + explncRNA2 × coef lncRNA2 + ... + explncRNAi × coef lncRNAi, and patients were categorized into high- and low-risk groups based on the median risk score. To verify if the SenLncSig risk score served as an independent prognostic factor, clinicopathological factors were included in both univariate and multivariate Cox regression analyses. The risk score level was employed to explore the distribution of living conditions. The model's accuracy was evaluated using the receiver operating characteristic (ROC) curve. Clinicopathological variables for the high and low-risk groups were depicted using the R package pheatmap, and the distribution of different risk scores among patients was analyzed using principal component analysis (PCA), with visualization provided by the R package scatterplot3d.

2.4. Construction of the nomogram

A nomogram that integrates risk scores and clinicopathological features was created using the R package rms to forecast 1, 3, and 5-year survival rates in LUAD patients. Calibration curves were utilized to assess the accuracy of the predicted survival against the actual survival outcomes.

2.5. Gene Set Enrichment Analysis (GSEA) of the senescence-related lncRNA predictive signature

Gene Set Enrichment Analysis (GSEA) was conducted on the high- and low-risk groups to discover distinct functional enrichments between them. Key biological processes and pathways were identified at significant levels, with a nominal p-value (NOM p) less than 0.05 and a false discovery rate (FDR) q-value less than 0.25. The findings were visualized using the R package ggplot2.

2.6. Estimation of immune infiltration

The proportion of immune cell infiltration and the activity of immune-related pathways in high- and low-risk LUAD samples were evaluated using single-sample GSEA (ssGSEA) (Rooney et al., 2015) and verified using the CIBERSORT algorithm (Newman et al., 2015) as a method of cross-validation. The Wilcoxon rank-sum test was applied to establish whether there was a significant difference in the proportions of immune cells between the low-risk and high-risk groups.

2.7. Potential relationship between the SenLncSig and immunotherapy, chemotherapy, and target therapy

Initially, the differential expression of 40 immune checkpoints was examined between the high-risk and low-risk groups (Wagner et al., 2021). Additionally, the tumor immune dysfunction and exclusion (TIDE, http://tide.dfci.harvard.edu/) module was utilized to differentiate potential responses to immunotherapy between these groups, predicting responses to anti-PD1 and anti-CTLA4 treatments based on pre-treatment transcriptional expression profiles of patient genomes (Yi et al., 2021). Moreover, to further assess the utility of SenLncSig in predicting LUAD's response to therapy, the half-maximal inhibitory concentrations (IC50) of common chemotherapeutic and targeted therapeutic drugs were calculated. The Wilcoxon signed-rank test and the R package pRRophetic were employed to analyze and display the differences in IC50 values between the high-risk and low-risk groups (Liu et al., 2020).

2.8. Statistical analysis

The Wilcoxon test was picked to analyze the expression differences of senescence-related DEGs between cancer and normal tissues. The Kaplan-Meier method along with the log-rank test were used to assess differences in overall survival (OS) rates between the high-risk and low-risk groups (Tang et al., 2021). The survivalROC package facilitated the generation of ROC curves and the calculation of the area under the curve (AUC). Group differences were evaluated using the Kruskal–Wallis test. Clinical data were examined either by the chi-square test or Fisher's exact test depending on the data characteristics (Huo et al., 2021). A Pearson correlation coefficient was utilized to assess the association between lncRNA expression, immune infiltration, and the expression of immune checkpoint genes. All statistical evaluations were conducted using R software (version 4.1.2).

3. Results

3.1. Enrichment analysis of senescence related DEGs in LUAD

Initially, the expression levels of 279 senescence-related genes in both tumor and normal tissues were analyzed to identify any abnormal expressions in the tumor tissues. Within LUAD tumor tissues, 23 out of 62 differentially expressed genes were found to be downregulated, while 39 were upregulated (Figures 1, 2). KEGG pathway analysis identified the top five enriched pathways as human T-cell leukemia virus one infection, cellular senescence, cell cycle, Kaposi sarcoma-associated herpesvirus infection, and p53 signaling pathway (Figure 3). On the other hand, GO analysis highlighted the most enriched categories as cell aging, aging, mitotic cell cycle phase transition, regulation of mitotic cell cycle phase transition, and cellular response to chemical stress (Figure 4). These results suggest that the DEGs predominantly play roles in cell senescence, the cell cycle, virus infection, cellular stress, and apoptosis.

3.2. Construction of the SenLncSig

Pearson correlation analysis revealed 1,081 lncRNAs linked to senescence, with 62 of these associated with the prognosis of LUAD (Figure 5). Furthermore, a set of seven senescence-related lncRNAs—AL031775.2, AC026355.1, AC090559.1, AL513550.1, C20orf197, AL365181.2 and AL606489.1—were identified through multivariate Cox regression analysis to create the SenLncSig prognostic signature. Figure 6 shows a heatmap illustrating the expression levels of the SenLncSig lncRNAs in LUAD patients. The senescence-related lncRNA-mRNA expression network was visualized using Cytoscape software (Figure 7, $|R^2| > 0.3$, $p < 0.001$). Based on the Sankey diagram in Figure 7, AL031775.2AC026355.1, AC090559.1, AL513550.1, C20orf197, AL365181.2 were identified as protective factors, whereas AL365181.2 and AL606489.1 were deemed risk factors.

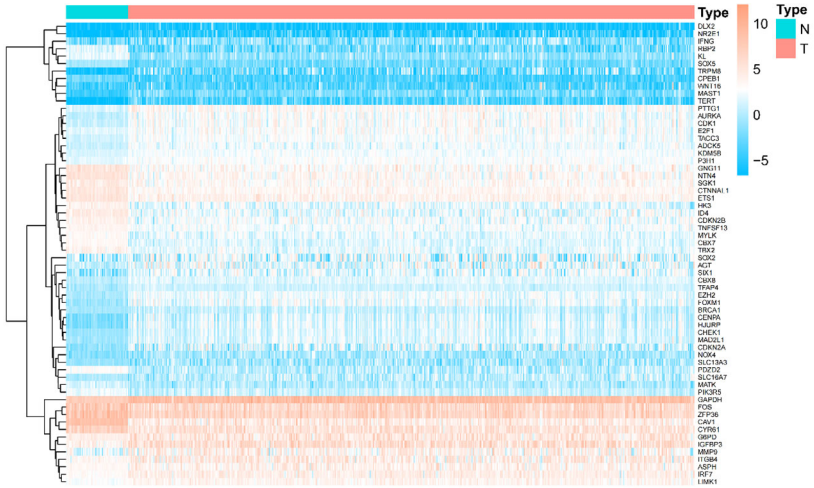

Figure 1. A heatmap displays 62 senescence DEGs between normal and LUAD tumor tissues.

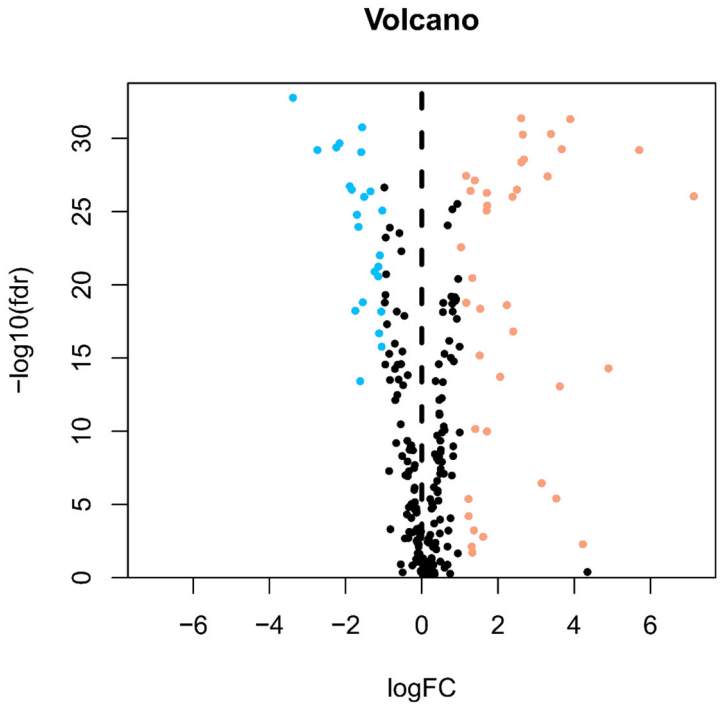

Figure 2. A volcano plot of senescence-related differentially expressed genes in lung adenocarcinoma.

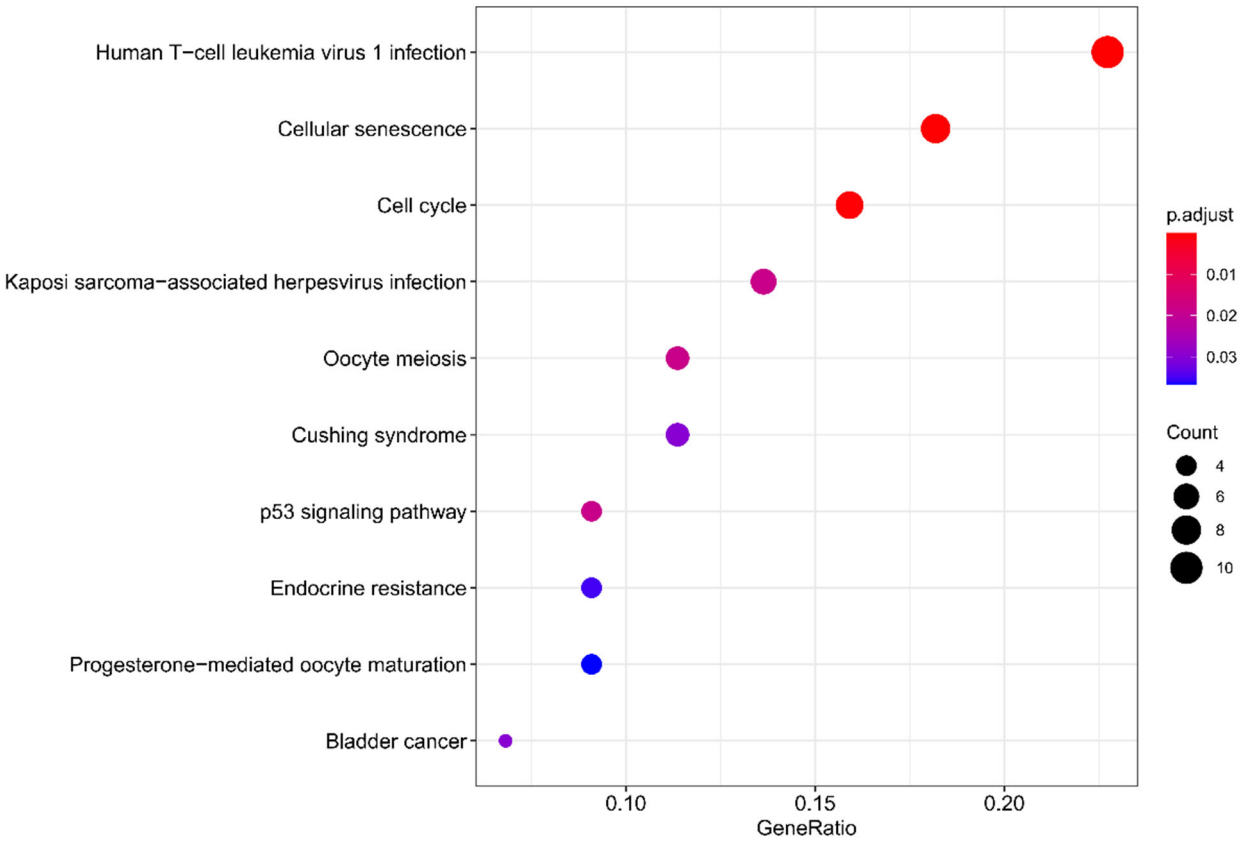

Figure 3. KEGG pathway enrichment analysis of senescence-related differentially expressed genes in lung adenocarcinoma.

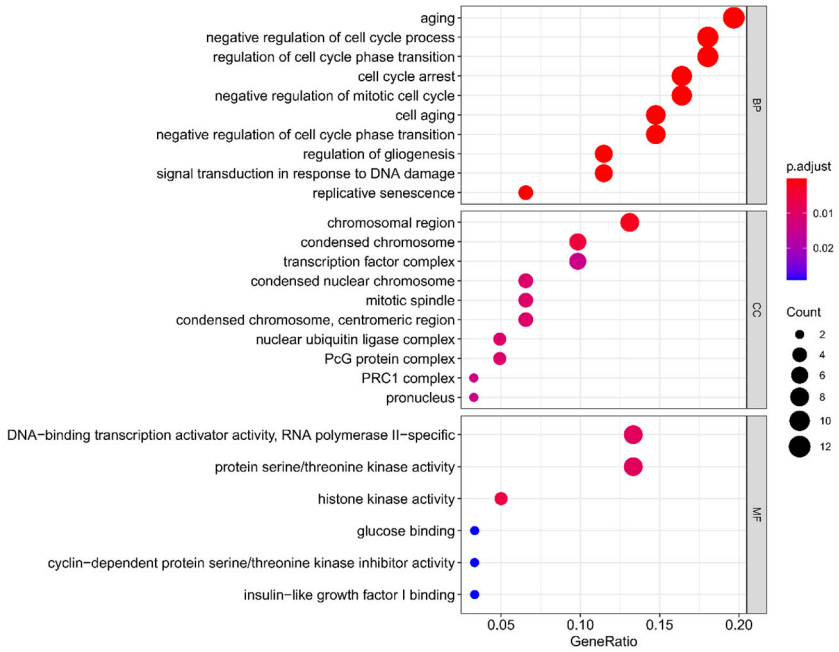

Figure 4. GO functional enrichment analysis of senescence-related differentially expressed genes in lung adenocarcinoma.

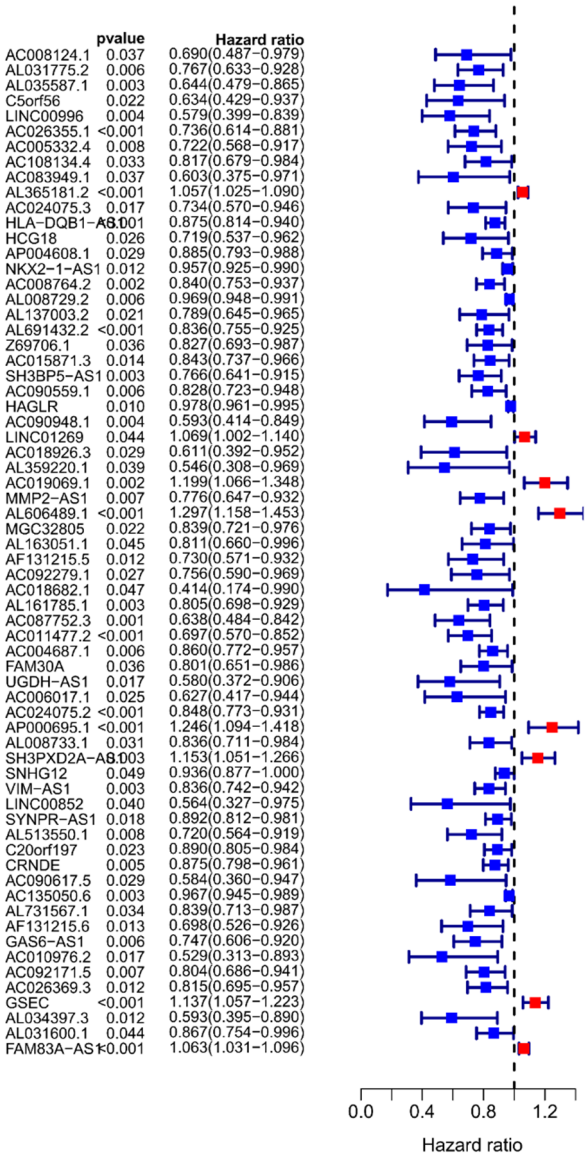

Figure 5. A forest plot shows the 62 senescence-related lncRNAs.

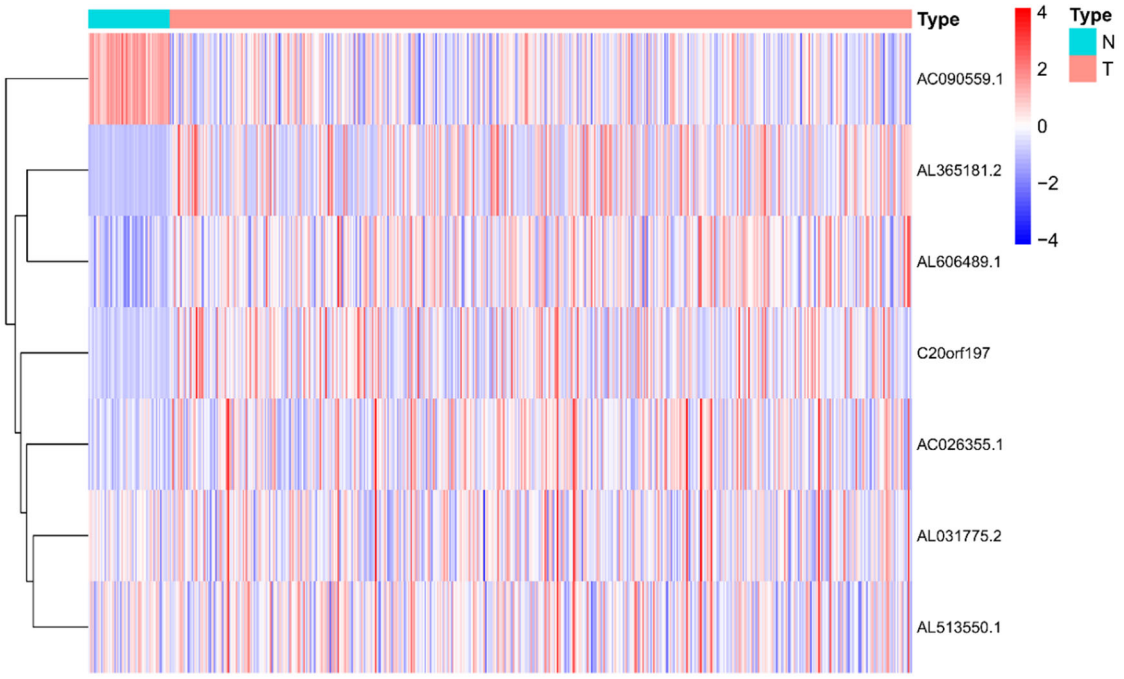

Figure 6. Expression levels of seven senescence-related lncRNAs associated with LUAD prognosis identified through multivariate Cox regression analysis.

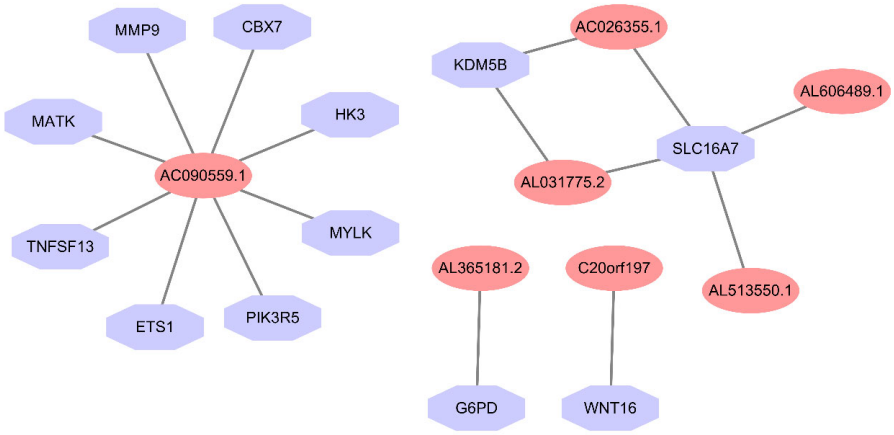

Figure 7. Co-expression network diagram of 12 senescence-related mRNAs and lncRNAs in lung adenocarcinoma.

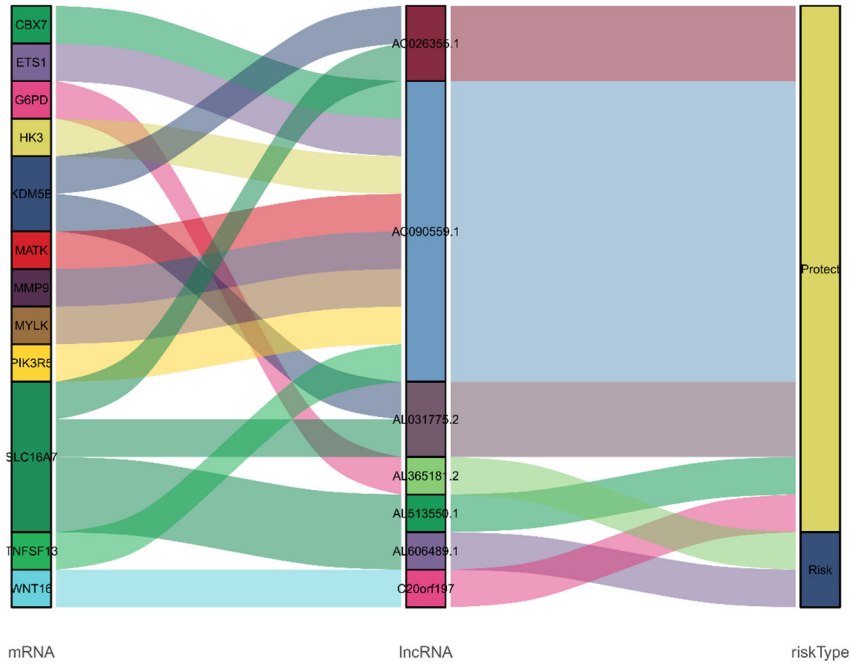

Figure 8. Sankey diagram of 12 senescence-related mRNAs and lncRNAs in lung adenocarcinoma.

3.3. Correlation between SenLncSig and prognosis of LUAD patients

The risk score of SenLncSig was calculated as follows: risk score = EXPgene(AL365181.2)*0.2587-EXPgene(AL031775.2)*0.5210-EXPgene(AC090559.1)*0.4512+EXPgene(AL606489.1)*0.4246-EXPgene(AL513550.1)*0.470-EXPgene(C20orf197)*0.30937. The formula was applied to compute each patient's risk score, and the patients were categorized into two groups according to the median risk score: a high-risk group (n = 256) and a low-risk group (n = 224) (Figure 9). Kaplan-Meier analysis revealed that overall survival (OS) was significantly shorter in the high-risk group compared to the low-risk group (Figure 9). Figures 10 and 11 illustrate the risk scores and survival data for individual patients, showing a higher number of deaths as risk scores increased. Both univariate and multivariate Cox regression analyses confirmed that the SenLncSig risk score was an independent prognostic indicator for LUAD (Figures 12,13), with an AUC of 0.797, making it the strongest predictor of LUAD prognosis among the clinicopathological variables studied (Figure 14). The AUC values for the 1-year, 3-year, and 5-year ROC curves were 0.731, 0.705, and 0.756, respectively, demonstrating that SenLncSig effectively predicts LUAD prognosis (Figure 15).

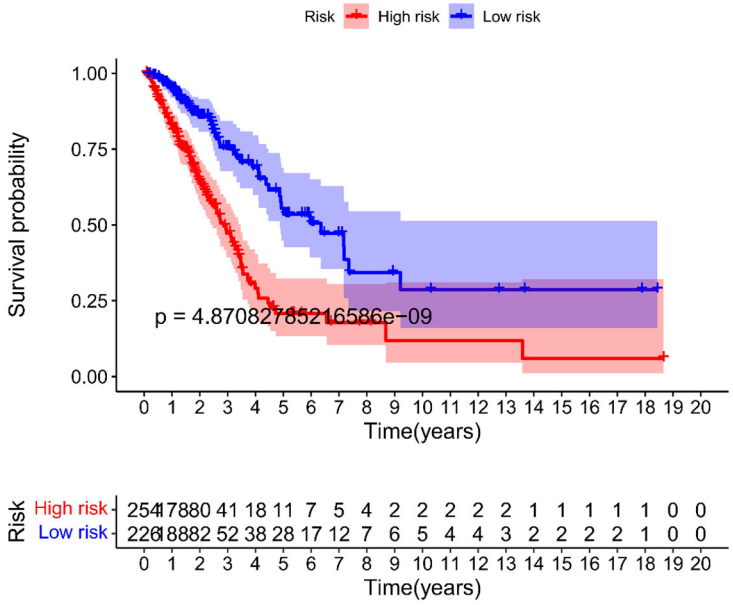

Figure 9. Kaplan-Meier survival curves for the high-risk and low-risk groups based on lung adenocarcinoma risk scores.

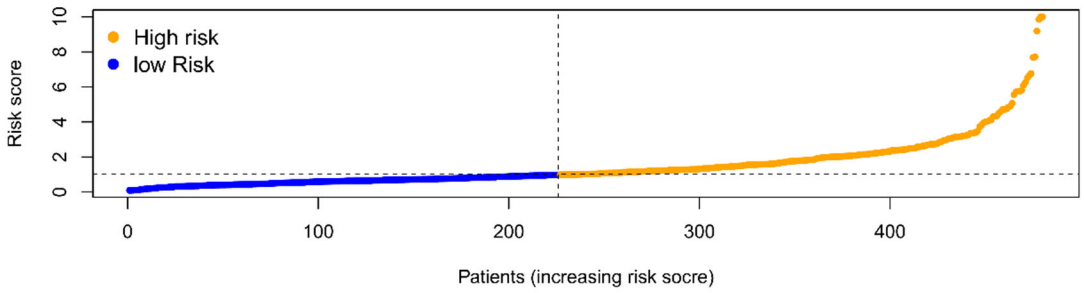

Figure 10. Risk score curves for the high and low-risk groups.

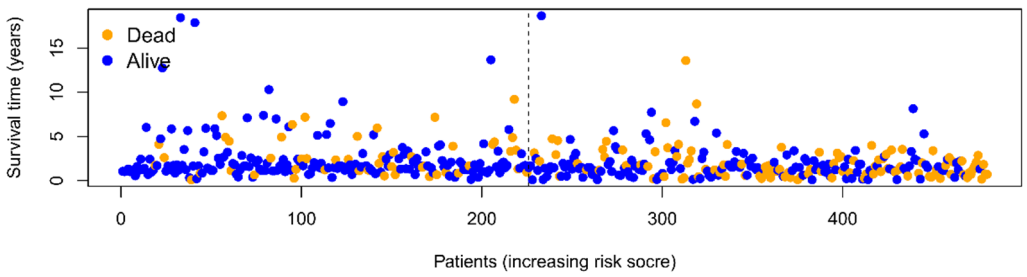

Figure 11. Survival statistics charts for the high and low-risk groups.

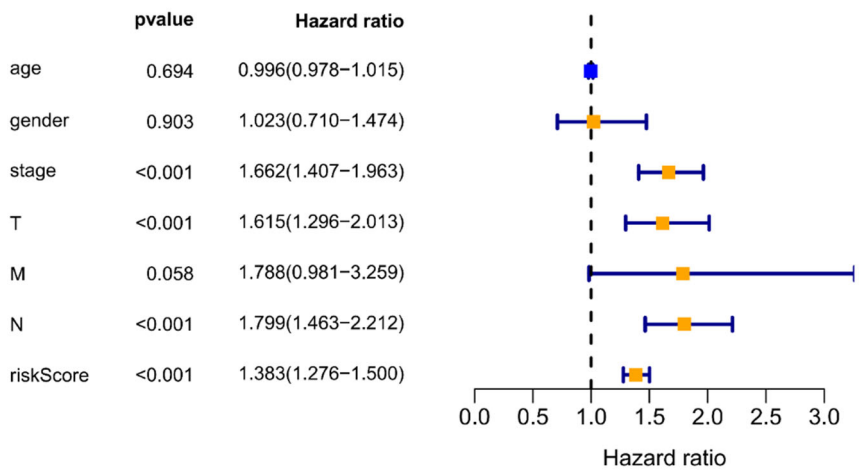

Figure 12. Forest plot of univariate Cox regression analysis for prognostic factors and risk scores in lung adenocarcinoma.

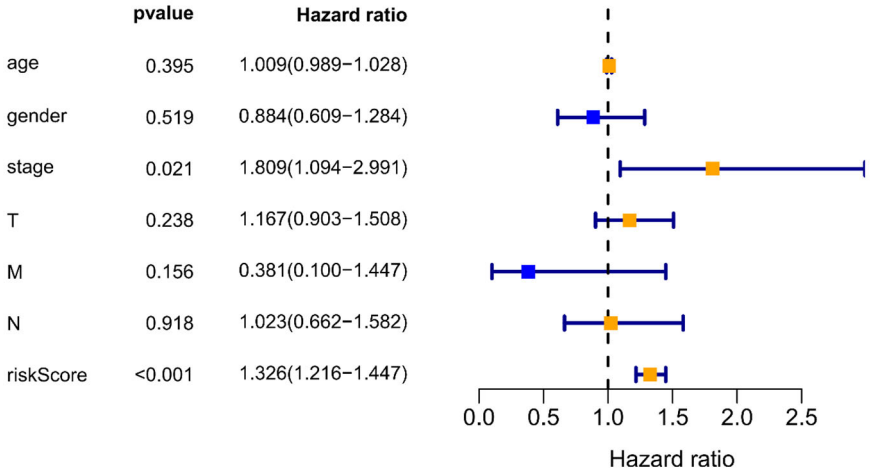

Figure 13. Forest plot of multivariate Cox regression analysis for clinical factors and risk scores in lung adenocarcinoma prognosis.

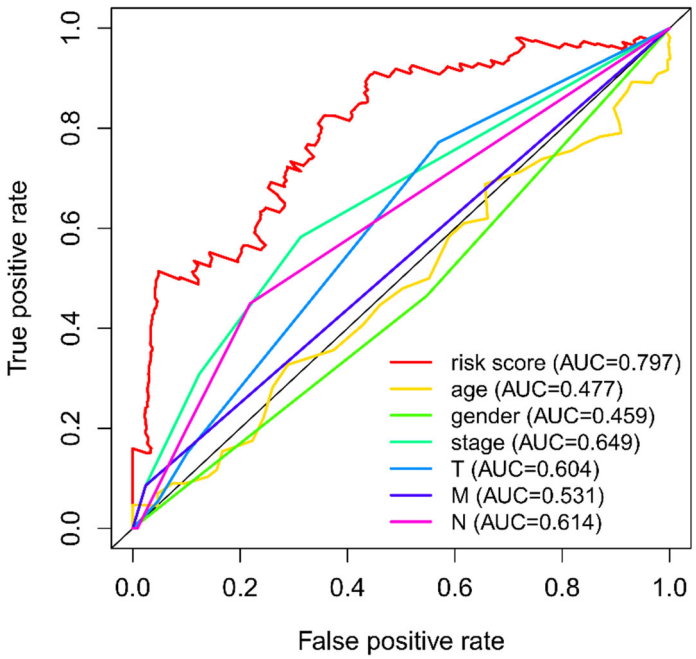

Figure 14. ROC curve of risk score and other clinical factors.

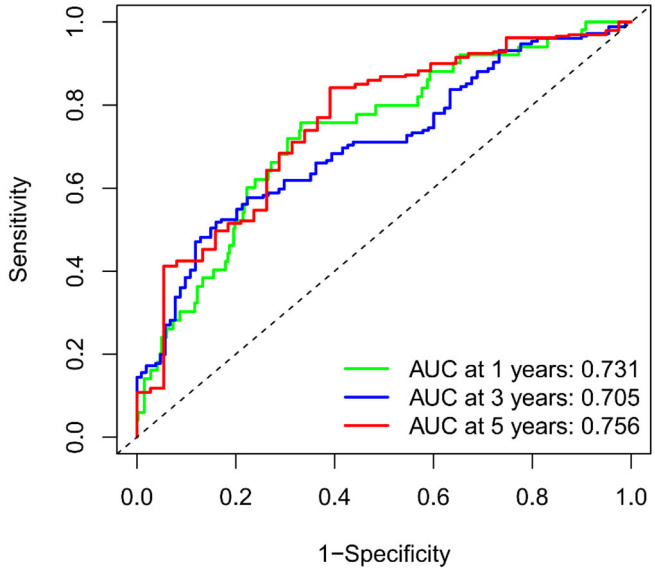

Figure 15. The ROC curves of the risk score at 1, 3, and 5 years.

Figure 16 illustrates the levels of expression of nine lncRNAs and clinicopathological factors within the SenLncSig model. Principal Component Analysis (PCA) was conducted on a genome-wide scale, senescence-related DEGs, senescence-related lncRNAs, and SenLncSig to discern between high-risk and low-risk patients (Figures 17A–D). The SenLncSig model effectively differentiated between low-risk and high-risk groups, as evidenced in Figure 17D, highlighting the precision of the model.

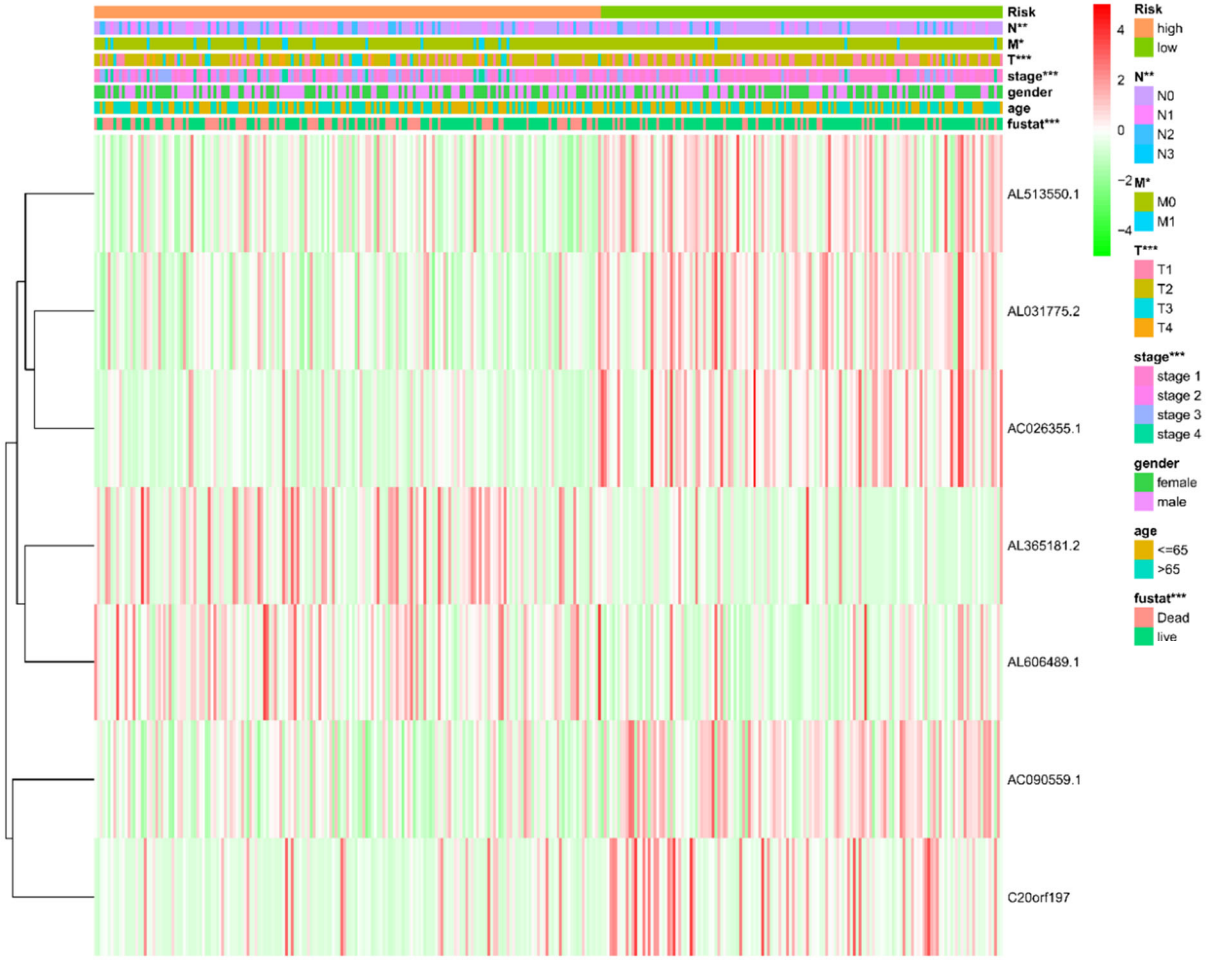

Figure 16. Heat map of the relationship between risk score and various clinical characteristic factors

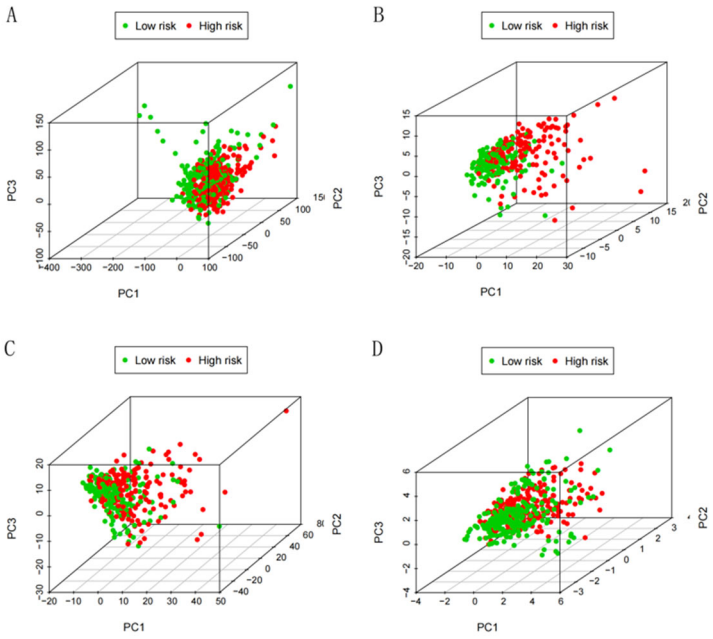

Figure 17. PCA of whole genome (A), cell aging related genes (B), cell aging related lncRNA (C), SenLncSig model (D)

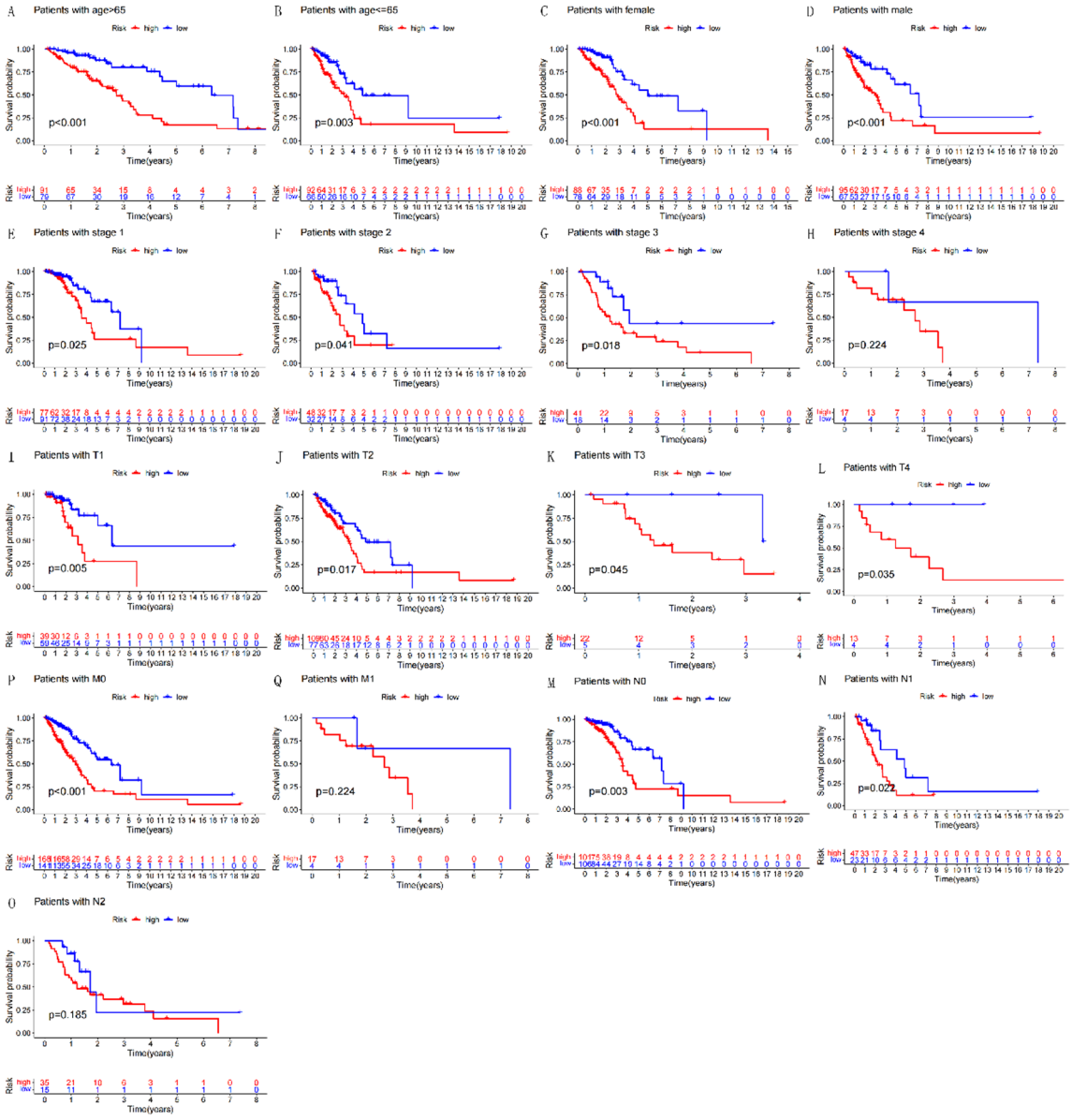

Figure 18. Kaplan–Meier survival curves for low and high risk groups classified based on clinicopathological variables. (A,B) Age; (C,D) Sex; (E,F) M stage; (G–I) N stage; (J–M) Overall stage; (N–Q) T stage. T, tumor; N, lymph node metastasis; M, distant metastasis.

Moreover, Figures 18A-Q illustrate the connection between clinical variables and the risk score. Notable associations were found between the risk score and factors such as age (both above and below 65 years, as shown in Figures 18A and B), gender (female and male, Figures 18C and D), M0 stage (Figure 18E), N0 and N1 stages (Figures 18G and H), overall TNM stages 2 and 3 (Figures 18K and L), and T2, T3, and T4 stages (Figures 18O-Q). The SenLncSig risk score was confirmed as an independent prognostic risk factor for LUAD patients.

3.4. Construction of the nomogram

A nomogram for clinical prognostic evaluation was developed using the LUADSenLncSig risk score along with other clinicopathological factors, aimed at predicting the survival likelihood at 1, 3, and 5 years for LUAD patients (Figure 19). According to three calibration plots, the mortality predicted by the nomogram closely matched the observed mortality rates (Figures 20A-C).

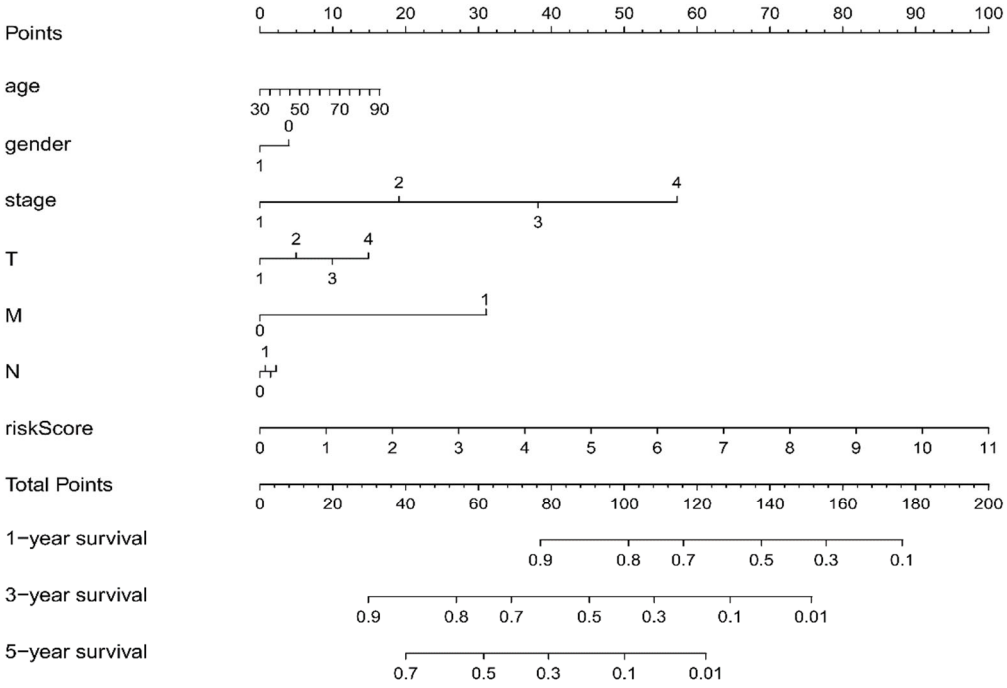

Figure 19. A nomogram constructed based on clinical characteristic factors and risk scores.

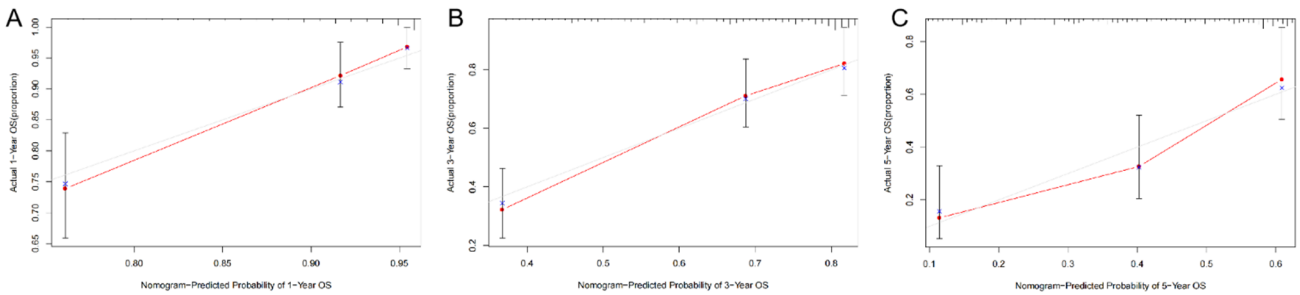

Figure 20. Calibration plots for 1, 3, and 5-year overall survival (OS) of lung adenocarcinoma patients obtained from the nomogram.

3.5. Internal validation of the SenLncSig

The TCGA-LUAD patient group, consisting of 480 individuals, was split into two internal validation cohorts, each containing 240 patients, to verify the universal applicability of SenLncSig to predicting overall survival (OS) in LUAD. The clinical details of the sample are provided in Table 1. In both the first and second internal cohorts, patients in the high-risk group exhibited shorter OS compared to those in the low-risk group (Figures 21A, C), aligning with the findings from the broader TCGA-LUAD dataset. Additionally, the area under the curve (AUC) for 1-year, 3-year, and 5-year survival was 0.77, 0.733, and 0.777 in the first internal cohort (Figure 21B) and 0.697, 0.678, and 0.735 in the second internal cohort (Figure 21D), respectively. These outcomes affirm the effectiveness of SenLncSig across both validation cohorts, underscoring the reliability of the predictive model.

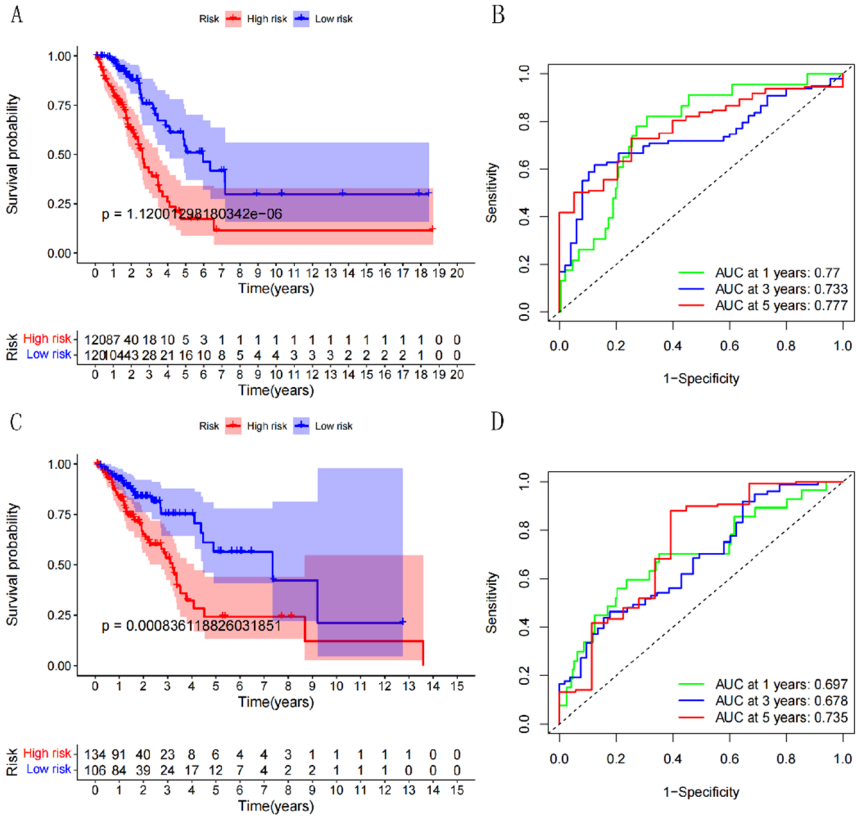

Figure 21. Kaplan-Meier curves and ROC curves for the two validation cohorts.

3.6. Identification of biological pathways associated with SenLncSig

Single GSEA enrichment analysis of the high-risk and low-risk groups, as distinguished by the model's risk scores, showed differential enrichment in KEGG signaling pathways and GO functions related to the expression of aging-associated lncRNAs. For KEGG signaling pathways, the high-risk group showed significant enrichment in five pathways: the cell cycle pathway (NES=2.15, NOM p<0.001, FDR q=0.008), oocyte meiosis pathway (NES=2.12, NOM p<0.001, FDR q=0.006), pentose phosphate pathway (NES=1.96, NOM p<0.001, FDR q=0.051), mismatch repair pathway (NES=1.95, NOM p<0.001, FDR q=0.041), and DNA replication pathway (NES=1.95, NOM p<0.001, FDR q=0.035). In the low-risk group, the most enriched pathways included hematopoietic cell lineage (NES=-1.89, NOM p=0.002, FDR q=0.152), autoimmune thyroid disease (NES=-1.87, NOM p=0.006, FDR q=0.096), intestinal immune network for IgA production (NES=-1.86, NOM p=0.008, FDR q=0.065), allograft rejection (NES=-1.85, NOM p=0.004, FDR q=0.056), and asthma (NES=-1.83, NOM p=0.014, FDR q=0.055) (Figure 22).

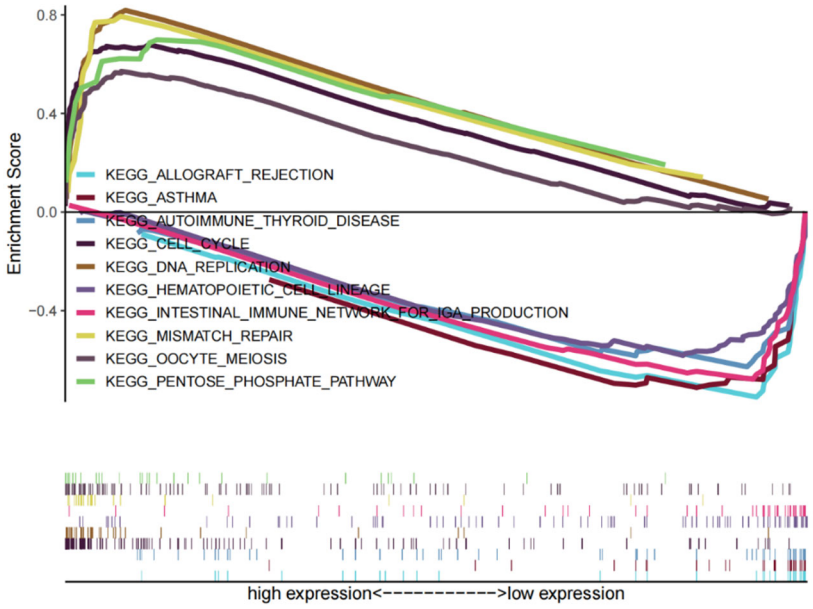

Figure 22. KEGG_GSEA enrichment analysis between high and low-risk groups.

For GO functions, in the high-risk group, the most enriched functions and biological processes include cadherin binding (NES=2.48, NOM p<0.001, FDR q<0.001), metaphase plate congression (NES=2.37, NOM p<0.001, FDR q<0.001), chromosome localization (NES=2.35, NOM p<0.001, FDR q<0.001), mitotic metaphase plate congression (NES=2.32, NOM p<0.001, FDR q=0.001), and microtubule cytoskeleton organization involved in mitosis (NES=2.31, NOM p<0.001, FDR q=0.001). In the low-risk group, the most enriched include the MHC class II biosynthetic process (NES=-2.02, NOM p<0.001, FDR q=0.998), peptidase activator activity involved in the apoptotic process (NES=-1.97, NOM p<0.001, FDR q=1.0), regulation of B cell receptor signaling pathway (NES=-1.97, NOM p=0.002, FDR q=0.690), negative regulation of TOR signaling (NES=-1.96, NOM p<0.001, FDR q=0.585), and negative regulation of phosphatidylinositol 3-kinase signaling (NES=-1.94, NOM p<0.001, FDR q=0.542) (Figure 23).

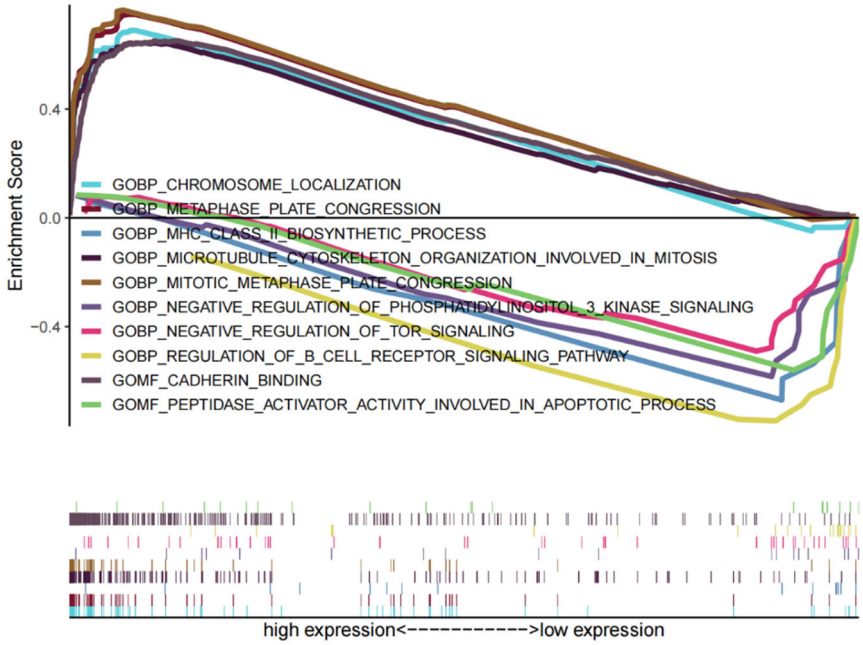

Figure 23. GO_GSEA enrichment analysis between high and low-risk groups.

3.7. Differential analysis of immune infiltration between high and low-risk groups.

To explore the impact of the quantity of immune cells in the tumor microenvironment on lung adenocarcinoma, we performed a differential analysis of immune infiltration using the ssGSEA method on the marker genes of most types of immune cells in high and low-risk groups. The differential analysis of immune cell quantities showed that the low-risk group had significantly higher numbers of anti-tumor immune cells such as immature dendritic cells (iDCs), mast cells, and helper T cells compared to the high-risk group (Figure 24). An analysis of the differences in immune functions between the high and low-risk groups revealed that scores for anti-tumor immune functions, including checkpoints, human leukocyte antigens (HLA), T cell co-inhibition, and T cell co-stimulation, were significantly higher in the low-risk group (Figure 25). These results suggest that the tumor microenvironment of lung adenocarcinoma patients in the low-risk group exhibits a stronger anti-tumor immune response compared to those in the high-risk group.

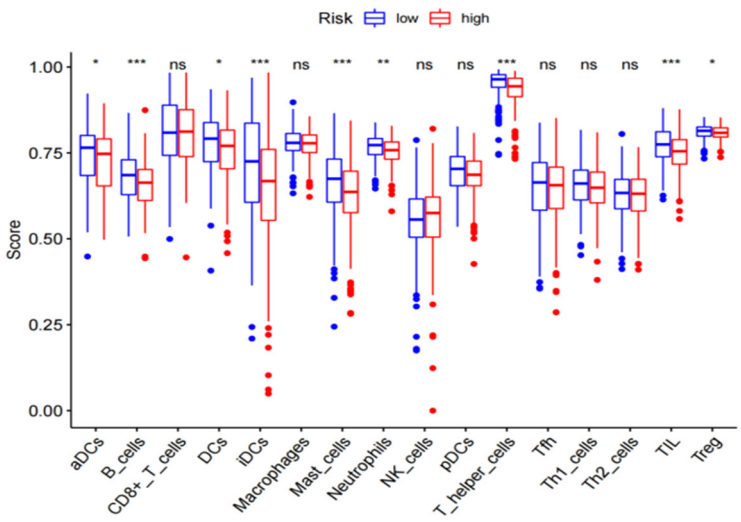

Figure 24. Immune cell count scores for high and low-risk groups.

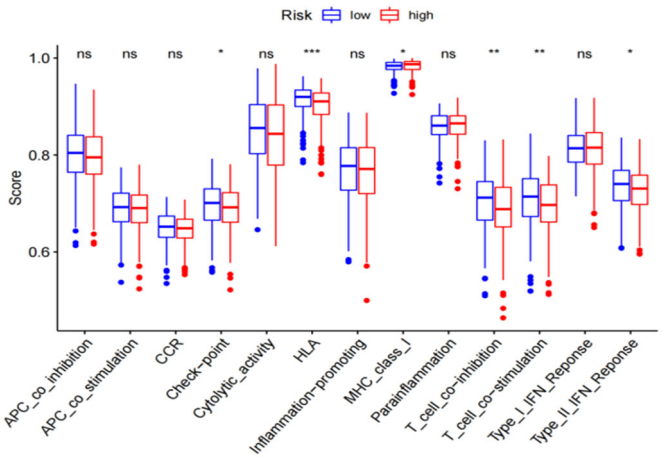

Figure 25. Immune function scores for high and low-risk groups.

To further validate the conclusions, we utilized the CIBERSORT algorithm to analyze and visualize the immune infiltration in the high and low-risk groups. The analysis of immune infiltration in the high and low-risk groups provided the content of immune cells in each sample (Figures 26 and 27). Subsequently, we performed a differential analysis of immune infiltration based on these results (Figure 28), which showed that the quantities of CD+8 T cells, M0 macrophages, and dendritic cells were significantly higher in the low-risk group compared to the high-risk group. This confirmed the results of the ssGSEA analysis and also indicated that both specific and non-specific immunity are suppressed in the high-risk group compared to the low-risk group.

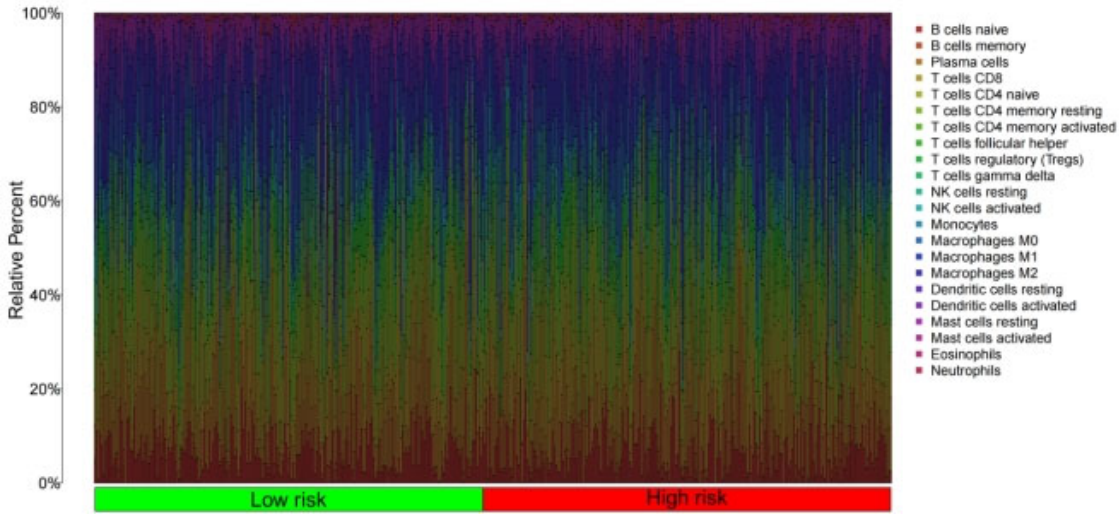

Figure 26. Proportion of various immune cells in high and low-risk groups.

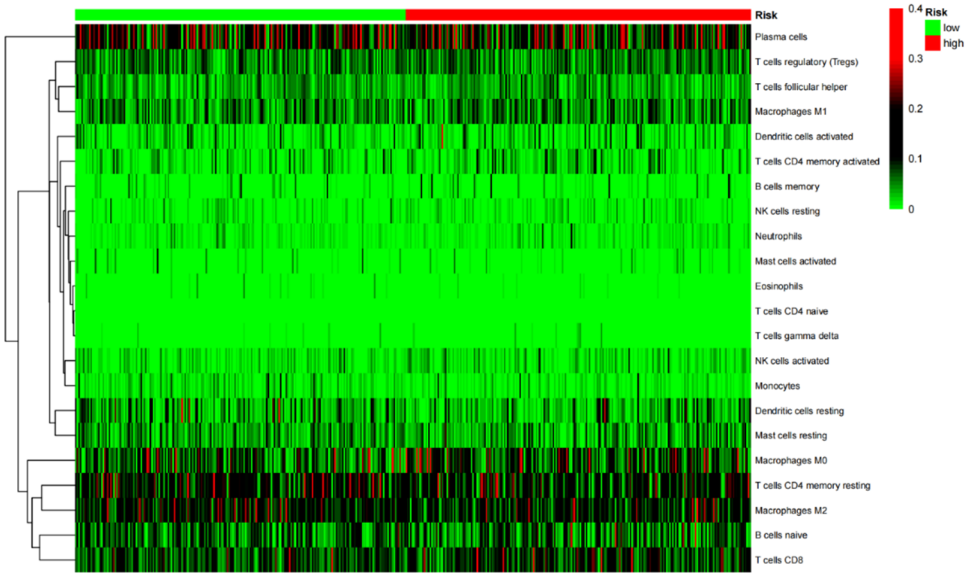

Figure 27. Heatmap of various immune cell expressions in high and low-risk groups.

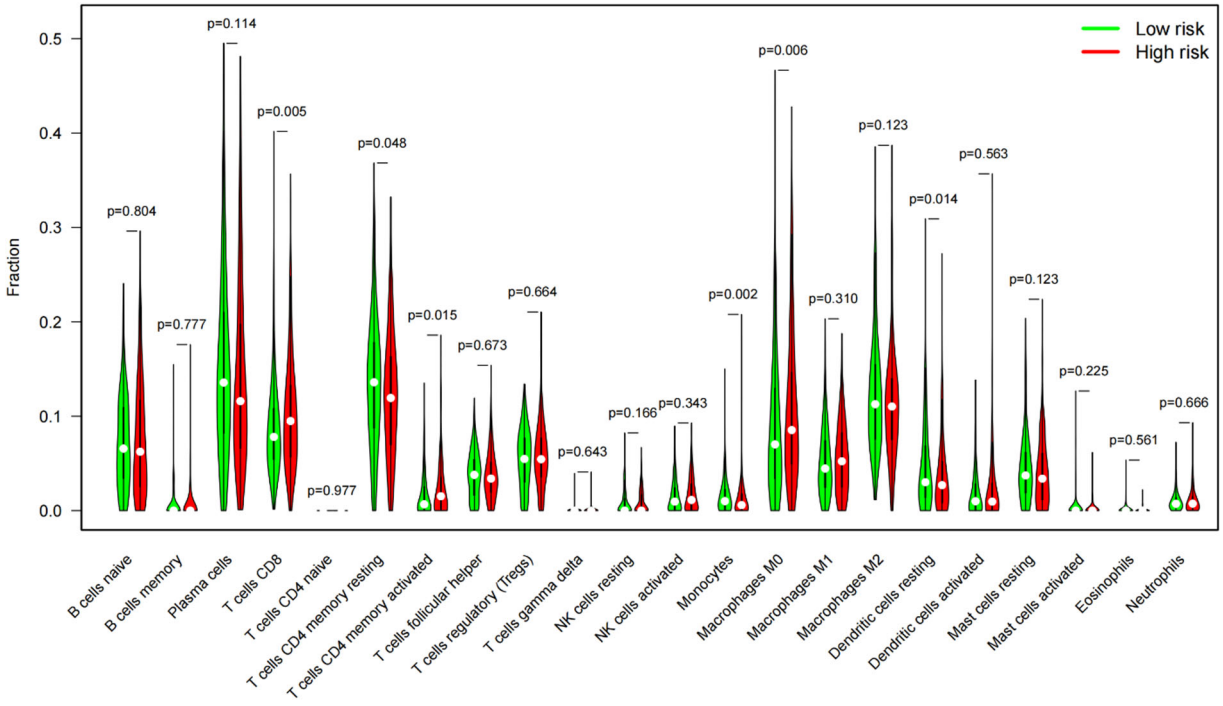

Figure 28. Differential analysis of immune infiltration between high and low-risk groups

3.8. Differential analysis of immune checkpoint expression between high and low-risk groups

Next, we compared the expression levels of 32 immune checkpoints in the high-risk and low-risk groups of the SenLncSig model and identified significant differences. The expression of immune therapy checkpoints currently widely used in clinical treatment and experimental exploration, such as CD40, HAVCR2, CD27, and BTLA, was significantly higher in the low-risk group (Figure 29). The results also show that the immune checkpoint expression levels are generally higher in the low-risk group compared to the high-risk group. This may indicate that these patients have a more active immune response, enabling their immune system to more effectively recognize and eliminate tumor cells, thereby inhibiting tumor growth and spread. This enhanced immune surveillance could be one reason for the better prognosis observed in low-risk patients. It may also suggest that low-risk group patients have more immune cell infiltration and a more active immune microenvironment, potentially responding better to immune checkpoint inhibitors such as PD-1, PD-L1, and CTLA-4 inhibitors.

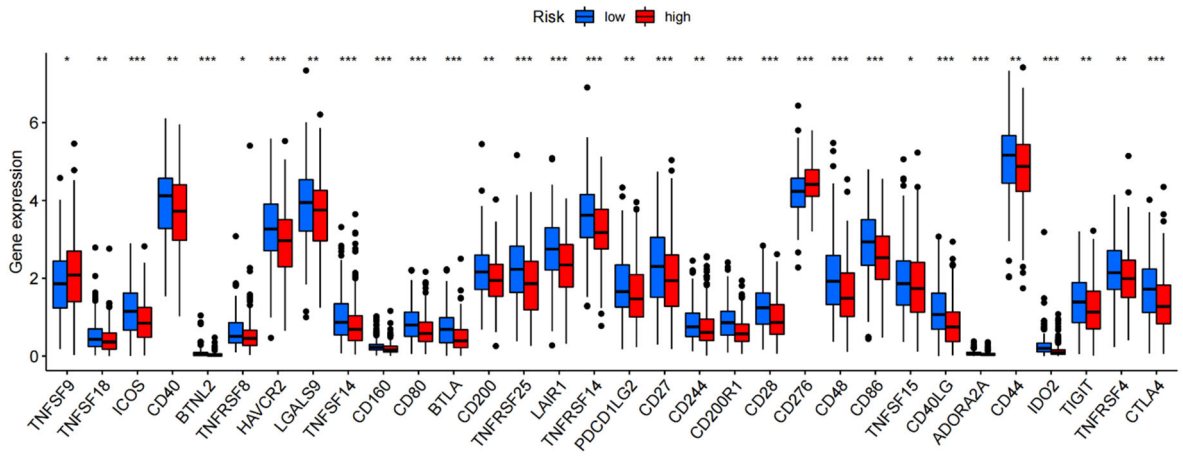

Figure 29. Expression levels of immune checkpoints in high and low-risk groups.

3.9. Analysis of the correlation between the SenLncSig model and the tumor microenvironment.

To determine if the risk scores of our constructed model are correlated with the tumor microenvironment, we used the ESTIMATE algorithm in R to score immune infiltration for high and low-risk groups distinguished by risk scores, and visualized the results (Figure 30). The figure shows that the low-risk group has higher stromal scores, immune scores, and the combined ESTIMATE scores than the high-risk group,

indicating that the prognosis of the low-risk group is better than that of the high-risk group, which is consistent with actual observations.

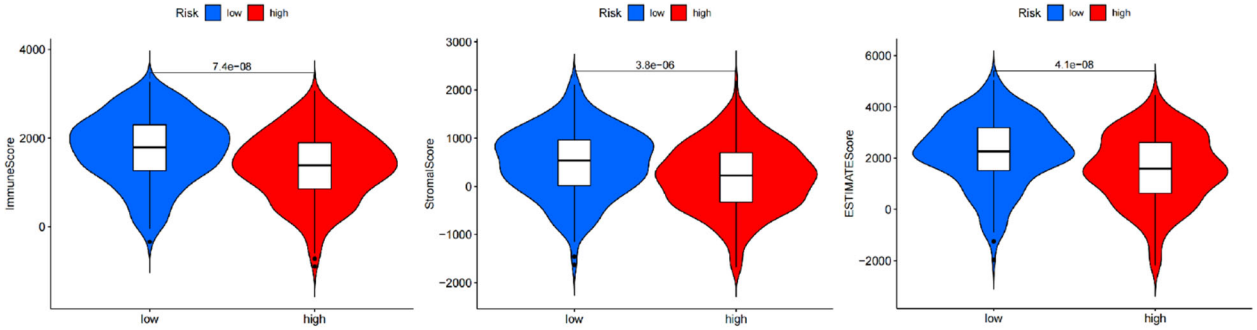

Figure 30. ESTIMATE algorithm immune infiltration scores for high and low-risk groups.

3.10. The relationship between SenLncSig risk scores and the efficacy of chemotherapy and targeted therapy for lung adenocarcinoma.

Finally, to help clinicians devise more precise treatment plans for patients, we analyzed the relationship between SenLncSig risk scores and the efficacy of chemotherapy and targeted therapy for lung adenocarcinoma, examining drug sensitivity in high and low-risk groups. Based on the results, and existing experiments and studies on drugs, we found that the targeted drug epidermal growth factor receptor (EGFR) inhibitor Erlotinib (Figure 31A); paclitaxel (Figure 31B); the experimental drug SGK1 inhibitor GSK650394 (Figure 31C); and the natural plant extract Parthenolide (Figure 31D) are more sensitive in the low-risk group with relatively lower IC50 values, indicating these drugs would achieve better efficacy in this group. Meanwhile, the chemotherapy drug methotrexate (Figure 32A); the broad-spectrum anticancer drug PAC-1 (Figure 32B); AKT inhibitor mk2206 (Figure 32C); and the multi-target tyrosine kinase inhibitor Ponatinib (AP.24534) (Figure 32D), are more sensitive in the high-risk group, suggesting these drugs may be more suitable for use in high-risk patients.

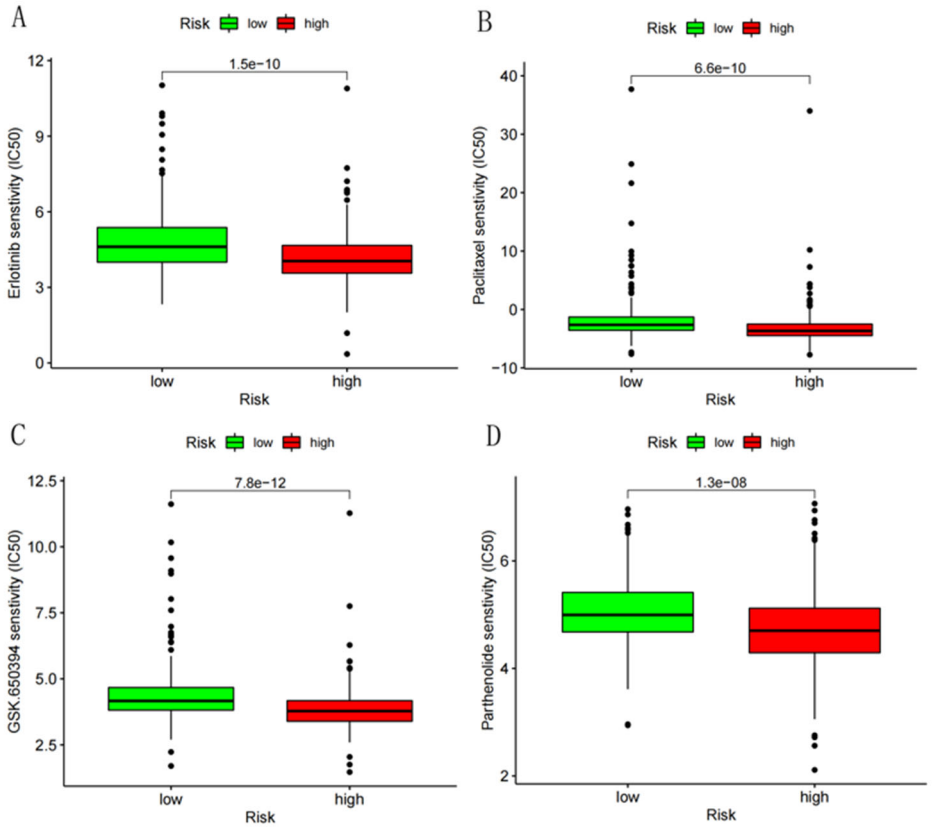

Figure 31. IC50 values of various targeted therapy drugs in high and low-risk patient groups.

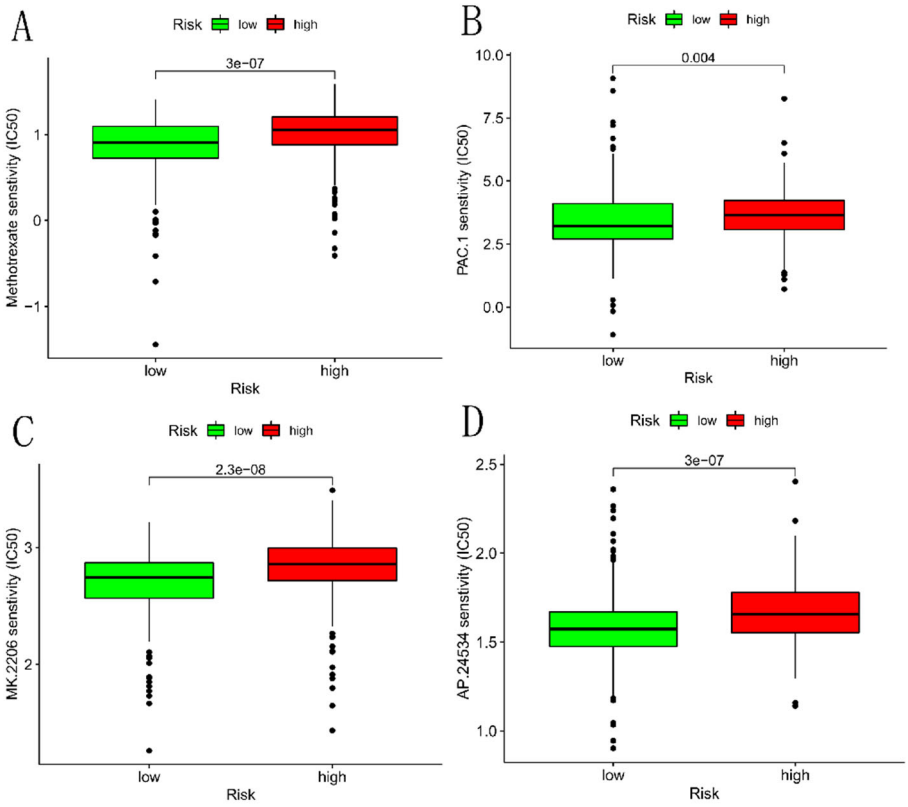

Figure 32. IC50 values of various targeted therapy drugs in high and low-risk patient groups.

4. Discussion

Lung cancer is the leading cause of cancer-related deaths worldwide. The Tumor Microenvironment (TME) refers to the local environment surrounding tumor cells, including non-tumor cells, the Extracellular Matrix (ECM), the vascular system, immune cells, and various cytokines and chemical signals. The tumor microenvironment plays a crucial role in the occurrence, development, metastasis, and response to treatment of tumors (Genova et al., 2022; Bonanno et al., 2018). The level of immune infiltration in the TME refers to the degree to which immune cells enter and exist within the tumor tissue. The TME is a complex ecosystem that includes tumor cells, immune cells, blood vessels, extracellular matrix, and other cell types. Within this environment, various components of the immune system, such as T cells, B cells, natural killer (NK) cells, macrophages, and dendritic cells, can penetrate the tumor tissue, forming immune infiltration. The level of immune infiltration is an important indicator for assessing the immune response status of tumors, which has significant implications for cancer treatment and prognosis (Peng et al., 2021; Wen et al., 2022).

Although chemotherapy and radiation therapy remain mainstream methods for many malignant tumors, Immune Checkpoint Inhibitors (ICIs) have now become indispensable in the treatment of various malignancies. During the progression of malignant tumors, the tumor immune response is often suppressed, and the core mechanism of ICIs is to lift the suppression on T cells, thereby activating an immune response against the tumor (Topalian et al., 2016). Additionally, ICIs also promote the activation of other cells in both the innate and adaptive immune systems, which work together to exert an anti-tumor effect (Wei et al., 2018). Changes in the immune response induced by ICIs can be observed not only in the tumor itself, nearby tissues, or distant organs such as draining lymph nodes and the circulatory system. This peripheral immune response is extremely critical for achieving positive clinical outcomes. Currently, three types of ICIs targeting different points have been clinically approved: PD-1 inhibitors, PD-L1 inhibitors, and CTLA-4 inhibitors. PD-1 is a protein on the surface of T cells, while PD-L1 is a protein on the surface of cancer cells. Their interaction can inhibit the activity of T cells. By using inhibitors targeting PD-1 (such as Nivolumab and Pembrolizumab) or PD-L1 (such as Atezolizumab and Durvalumab), this interaction can be blocked, enhancing the immune system's attack on cancer cells (Jenkins et al., 2018). CTLA-4 is another protein on the surface of T cells that can inhibit T cell activation. Inhibitors targeting CTLA-4 (such as Ipilimumab) can prevent this inhibitory effect and promote the activity of the immune system (Pennock & Chow, 2015).

Although ICIs represent the most profound and advanced treatment mechanisms at this stage, they are limited by the possibility of over-activating the immune system, which may attack the body's own tissues, leading to the occurrence of immune-related side effects. Therefore, only a small portion of patients benefit from ICI treatments, and the overall efficacy rate is less than 20%. Thus, fully assessing whether patients can benefit from ICI treatment is the first step in formulating a clinical treatment plan for patients.

Recently, the U.S. Food and Drug Administration (FDA) approved immune checkpoint inhibitors (ICIs) for the treatment of lung adenocarcinoma, changing the selection of clinical treatment methods (Wu et al., 2022). However, the overall efficacy rate of ICIs is less than 20%, with only a minority of lung adenocarcinoma patients benefiting from ICI therapy. Therefore, a comprehensive assessment of whether patients benefit from ICI treatment is crucial. Biomarkers provide decision-making information for this treatment, but currently, there are no effective biomarkers for predicting

clinical efficacy. PD-L1 detected by tumor cell immunohistochemistry (IHC) is the standard biomarker for predicting the effectiveness of ICI therapy. In patients with advanced non-small cell lung cancer (NSCLC), pembrolizumab has been used as a first-line treatment, with a PD-L1 expression threshold of 50% (Shiravand et al., 2022). However, PD-L1 expression is low in some patients and there are false-negative results, as well as spatial differences within and outside the tumor. Moreover, compared to a single clinical biomarker, combining multiple biomarkers into a single model can improve predictive accuracy, helping to tailor precise individual treatment plans (Twomey & Zhang, 2021).

Cellular senescence has recently been identified as an important cellular function type within the tumor microenvironment, including in lung adenocarcinoma. Recently, it has been discovered that some lncRNAs are involved in the regulation of cellular senescence in lung adenocarcinoma patients; however, the overall pattern of LUAD cellular senescence regulation networks remains largely unknown (Liu et al., 2023). Therefore, we developed a SenLncSig signature to predict aging and prognosis in lung adenocarcinoma. Validated and assessed, the SenLncSig model developed in this study has good predictive performance for the prognosis of TCGA-LUAD samples. Additionally, including the SenLncSig risk score, a nomogram could potentially guide clinical decision-making. Notably, SenLncSig can stratify LUAD patients based on the expression levels of immune checkpoint genes, which is very important for helping patients select drugs and therapies that may benefit them (Degirmenci & Lei, 2016).

This study is notable for exploring the association between cellular senescence and the prognosis of lung adenocarcinoma and the tumor microenvironment (Lin et al., 2021). Currently, the role of cellular senescence and the tumor microenvironment combined in tumors is often overlooked in preclinical studies, which are usually designed for young mice rather than old mice. This might help explain why many successful preclinical responses fail to replicate when entering actual clinical trials. When considering the roles and mechanisms of network-related genes in lung adenocarcinoma tissue in comprehensive cancer treatment, cellular senescence should be considered a parameter (Liu et al., 2022).

In this study, we also identified the relationship between the SenLncSig model derived from aging genes and the potential efficacy in lung adenocarcinoma. Based on the stratification of lung adenocarcinoma SenLncSig, the expression of most immune checkpoints, immune pathway activation, and anti-tumor immune cell infiltration are all higher in the low-risk group, suggesting that low-risk patients may benefit more from immunotherapy (Montes et al., 2021). Moreover, compared to other studies that used the TCGA database to develop lncRNA prognostic models, our SenLncSig model has higher reliability. This suggests that senescent cells in the tumor microenvironment, along with other biomarkers, are equally important in predicting the prognosis of lung adenocarcinoma and assessing the effectiveness of immune therapy. Interestingly, other studies have also focused on the role of senescence-associated long non-coding RNAs in different cancers, including liver cancer, colorectal cancer, and gastric cancer (Peng et al., 2017; Kim et al., 2017). These studies' AUC values are similar to the time-dependent ROC curves of our model and specifically highlight the significant contribution of senescent cells to the tumor microenvironment.

It must be admitted that this study still has some areas where it is not rigorous enough from design to execution. First, there is a need to consider using more external data to assess whether the SenLncSig model fully matches other datasets. Second, the lack of some key data points, such as the situation of patients who have received second-line treatment, which cannot be included in the diagnostic charts, might affect the accuracy of the model. Third, functional studies are needed to better understand the molecular mechanisms of effects related to senescence-associated lncRNAs.

In summary, we have developed a lncRNA risk score model named SenLncSig, which can be used to predict the prognosis of lung adenocarcinoma. Notably, SenLncSig is associated with levels of immune cell infiltration and the potential effects of tumor immunotherapy. These results highlight the potential future direction of tumor immunotherapy focused on cellular senescence. Moreover, as sequencing technologies become more widely available and cost-effective, bulk sequencing as a technique may be more readily introduced into clinical practice and become a standard management approach.

5. Data Availability Statement

The study's original contributions are detailed in the article and Supplementary Material. For additional questions, please contact the corresponding author.

6. Author Contributions

YK and LY initiated the study and its design, also offering administrative assistance. YK were involved in data analysis, and they wrote, reviewed, and edited the manuscript. YK and LB aided in analyzing data and reviewed the manuscript. All authors have read and given their approval to the final manuscript. Every author contributed to the article and agreed on the version submitted for publication.

Acknowledgment

The authors express their appreciation to The Cancer Genome Atlas (TCGA) for providing valuable RNA sequence data complete with detailed clinical information (https://tcga-data.nci.nih.gov/tcga/). They also extend their gratitude to BioMed Proofreading® LLC Co., Ltd. and the developers of the R language for their contributions to building bioinformatics analysis techniques, which serve as fundamental tools for conducting bioinformatics analysis.

References

[1] Avelar, R. A., Ortega, J. G., Tacutu, R., Tyler, E. J., Bennett, D., & Binetti, P. (2020). A multidimensional systems biology analysis of cellular senescence in aging and disease. Genome Biology, 21, 91.

[2] Bonanno, L., Pavan, A., Dieci, M. V., Di Liso, E., et al. (2018). The role of immune microenvironment in small-cell lung cancer: distribution of PD-L1 expression and prognostic role of FOXP3-positive tumour infiltrating lymphocytes. European Journal of Cancer.

[3] Bray, F., Ferlay, J., Soerjomataram, I., Siegel, R. L., Torre, L. A., & Jemal, A. (2018). Global cancer statistics 2018: GLOBOCAN estimates of incidence and mortality worldwide for 36 cancers in 185 countries. CA: A Cancer Journal for Clinicians, 68(6), 394-424.

[4] Campisi, J. (2013). Aging, cellular senescence, and cancer. Annual Review of Physiology, 75, 685-705.

[5] Degirmenci, U., Lei, S. (2016). Role of lncRNAs in cellular aging. Frontiers in Endocrinology.

[6] Do, H., & Kim, W. (2018). Roles of oncogenic long non-coding RNAs in cancer development. Genomics & Informatics, 16(1), e18.

[7] Genova, C., Dellepiane, C., Carrega, P., et al. (2022). Therapeutic implications of tumor microenvironment in lung cancer: focus on immune checkpoint blockade. Frontiers in Immunology.

[8] Hoang, P. H., & Landi, M. T. (2022). DNA methylation in lung cancer: mechanisms and associations with histological subtypes, molecular alterations, and major epidemiological factors. Cancers, 14(4), 961.

[9] Huo, J., Wu, L., Zang, Y., Dong, H., Liu, X., He, F., & Zhang, X. (2021). Eight-gene metabolic signature related with tumor-associated macrophages predicting overall survival for hepatocellular carcinoma. BMC Cancer, 21, 77.

[10] Jenkins, R. W., Barbie, D. A., Flaherty, K. T. (2018). Mechanisms of resistance to immune checkpoint inhibitors. British Journal of Cancer.

[11] Jin, D., Song, Y., Chen, Y., & Zhang, P. (2020). Identification of three lncRNAs as potential predictive biomarkers of lung adenocarcinoma. BioMed Research International, 2020, Article 7573689.

[12] Kim, C., Kang, D., Lee, E. K., Lee, J. S. (2017). Long noncoding RNAs and RNA-binding proteins in oxidative stress, cellular senescence, and age-related diseases. Oxidative Medicine and Cellular Longevity.

[13] Lecot, P., Alimirah, F., Desprez, P. Y., Campisi, J., & Wiley, C. D. (2016). Context-dependent effects of cellular senescence in cancer development. British Journal of Cancer, 114(11), 1180-1184.

[14] Lin, W., Wang, X., Xu, Z., Wang, Z., Liu, T., Cao, Z., et al. (2021). Identification and validation of cellular senescence patterns to predict clinical outcomes and immunotherapeutic responses in lung adenocarcinoma. Cancer Cell International.

[15] Liu, A., Wang, X., Hu, L., Yan, D., Yin, Y., Zheng, H., Liu, G. et al. (2023). A predictive molecular signature consisting of lncRNAs associated with cellular senescence for the prognosis of lung adenocarcinoma. Plos One.

[16] Liu, H., Zhao, H., Sun, Y. (2022). Tumor microenvironment and cellular senescence: Understanding therapeutic resistance and harnessing strategies. Seminars in Cancer Biology.

[17] Liu, J., Nie, S., Wu, Z., Jiang, Y., Wan, S., Li, S., Meng, H. (2020). Exploration of a novel prognostic risk signatures and immune checkpoint molecules in endometrial carcinoma microenvironment. Genomics.

[18] Miranda-Filho, A., Piñeros, M., Ferlay, J., Soerjomataram, I., Monnereau, A., & Bray, F. (2019). Epidemiology and patterns of care for invasive breast and cervical cancer in 57 low- and middle-income countries: a population-based study. The Lancet Global Health, 7(7), e951-e961.

[19] Montes, M., Lubas, M., Arendrup, F. S., Mentz, B., et al. (2021). The long non-coding RNA MIR31HG regulates the senescence associated secretory phenotype. Nature Communications.

[20] Muppa, P., Terra, S. B. S. P., Sharma, A., Mansfield, A. S., et al. (2019). Immune cell infiltration may be a key determinant of long-term survival in small cell lung cancer. Journal of Thoracic Oncology.

[21] Newman, A. M., Liu, C. L., Green, M. R., Gentles, A. J., Feng, W., Xu, Y., ... & Alizadeh, A. A. (2015). Robust enumeration of cell subsets from tissue expression profiles. Nature Methods, 12(5), 453-457.

[22] Peng, C., Hu, W., Weng, X., Tong, R., Cheng, S., Ding, C., et al. (2017). Over expression of long non-coding RNA PANDA promotes hepatocellular carcinoma by inhibiting senescence associated inflammatory factor IL8. Scientific Reports.

[23] Peng, H., Wu, X., Zhong, R., Yu, T., Cai, X., Liu, J., et al. (2021). Profiling tumor immune microenvironment of non-small cell lung cancer using multiplex immunofluorescence. Frontiers in Immunology.

[24] Pennock, G. K., Chow, L. Q. M. (2015). The evolving role of immune checkpoint inhibitors in cancer treatment. The Oncologist.

[25] Rooney, M. S., Shukla, S. A., Wu, C. J., Getz, G., & Hacohen, N. (2015). Molecular and genetic properties of tumors associated with local immune cytolytic activity. Cell, 160(1-2), 48-61.

[26] Schosserer, M., Grillari, J., & Breitenbach, M. (2017). The dual role of cellular senescence in developing tumors and their response to cancer therapy. Frontiers in Oncology, 7, 278.

[27] Serviss, J. T., Johnsson, P., & Grandér, D. (2014). An emerging role for long non-coding RNAs in cancer metastasis. Frontiers in Genetics, 5, 234.

[28] Shi, L., Ginn, L., La Montagna, M., & Garofalo, M. (2020). LncRNAs in non-small-cell lung cancer. Non-coding RNA, 6(3), 25.

[29] Shiravand, Y., Khodadadi, F., Kashani, S.M.A. (2022). Immune checkpoint inhibitors in cancer therapy. Current Oncology Reports.

[30] Silva, A., Bullock, M., & Calin, G. (2015). The clinical relevance of long non-coding RNAs in cancer. Cancers, 7(4), 884.

[31] Tang, P., Qu, W., Wang, T., Liu, M., Wu, D., & Tan, L. (2021). Identifying a hypoxia-related long non-coding RNAs signature to improve the prediction of prognosis and immunotherapy response in hepatocellular carcinoma. Frontiers in Genetics, 12, 785185.

[32] Topalian, S. L., Taube, J. M., Anders, R. A., et al. (2016). Mechanism-driven biomarkers to guide immune checkpoint blockade in cancer therapy. Nature Reviews Cancer.

[33] Twomey, J.D., Zhang, B. (2021). Cancer immunotherapy update: FDA-approved checkpoint inhibitors and companion diagnostics. The AAPS Journal.

[34] Wagner, M., Jasek, M., Karabon, L. (2021). Immune checkpoint molecules—inherited variations as markers for cancer risk. Frontiers in Immunology.

[35] Wei, S. C., Duffy, C. R., Allison, J. P. (2018). Fundamental mechanisms of immune checkpoint blockade therapy. Cancer Discovery.

[36] Wen, S., Peng, W., Chen, Y., Du, X., Xia, J., Shen, B., Zhou, G. (2022). Four differentially expressed genes can predict prognosis and microenvironment immune infiltration in lung cancer: a study based on data from the GEO. BMC Cancer.

[37] West, L., Vidwans, S. J., Campbell, N. P., Shrager, J., Simon, G. R., Bueno, R., ... & Chen, H. (2012). A novel classification of lung cancer into molecular subtypes. PLoS One, 7(2), e31906.

[38] Wu, Q., Qian, W., Sun, X., Jiang, S. (2022). Small-molecule inhibitors, immune checkpoint inhibitors, and more: FDA-approved novel therapeutic drugs for solid tumors from 1991 to 2021. Journal of Hematology & Oncology.

[39] Xu, X., Zhou, X., Chen, Z., Gao, C., Zhao, L., & Cui, Y. (2020). Silencing of lncRNA XIST inhibits non-small cell lung cancer

growth and promotes chemosensitivity to cisplatin. Aging (Albany NY), 12(5), 6720-6737.

[40] Yi, M., Li, A., Zhou, L., Chu, Q., Luo, S., Wu, K. (2021). Immune signature-based risk stratification and prediction of immune checkpoint inhibitor's efficacy for lung adenocarcinoma. Cancer Immunology Research.

[41] Yuan, S., Xiang, Y., Guo, X., Zhang, C., Li, C., & Xie, M. (2020). Circulating long noncoding RNAs act as diagnostic biomarkers in non-small cell lung cancer. Frontiers in Oncology, 10, Article 537120.

[42] Zhang, X. Z., Liu, H., & Chen, S. R. (2020). Mechanisms of long non-coding RNAs in cancers and their dynamic regulations. Cancers, 12(5), 1245.